Outstanding Nobility Observed in Cu_5 Clusters Reveals the Key Role of Collective Quantum Effects

David Buceta, Shahana Huseyinova, Miguel Cuerva, Héctor Lozano, Lisandro J. Giovanetti, José M. Ramallo-López, Patricia López-Caballero, Alexander Zanchet, Alexander O. Mitrushchenkov, Andreas W. Hauser, Giampaolo Barone, Cristián Huck-Iriart, Carlos Escudero, Juan Carlos Hernández-Garrido, José Juan Calvino, Miguel López-Haro, María Pilar de Lara-Castells, Félix G. Requejo,* M. Arturo López-Quintela**

D. Buceta, S. Huseyinova, M. Cuerva, Héctor Lozano, M. A. López-Quintela
Department of Physical Chemistry, Nanomag Laboratory, Universidad de Santiago de Compostela, E-15782 Santiago de Compostela, Spain
Email Address: malopez-quintela@usc.es

L. J. Giovanetti, J. M. Ramallo-López, F. G. Requejo
Instituto de Investigaciones Fisicoquímicas Teóricas y Aplicadas (INIFTA), Dto. de Química, Facultad de Ciencias Exactas, UNLP and CONICET. Diag 113 y 64. 1900 La Plata, Argentina
Email Address: requejo@inifta.unlp.edu.ar

P. López-Caballero, A. Zanchet, M. P. de Lara-Castells
Instituto de Física Fundamental (AbinitSim Unit), CSIC, Serrano 123, 28006 Madrid, Spain
Email Address: Pilar.deLara.Castells@csic.es

A. Zanchet
Dpto. de Química Física, Facultad de Química, Universidad de Salamanca, Salamanca, Spain

A. O. Mitrushchenkov
MSME, Univ Gustave Eiffel, UPEC, CNRS, F-77454, Marne-la-Vallée, France

A. W. Hauser
Graz University of Technology, Institute of Experimental Physics, Petersgasse 16, 8010 Graz, Austria

G. Barone
Department of Biological, Chemical and Pharmaceutical Sciences and Technologies, University of Palermo, 90128 Palermo, Italy

C. Huck-Iriart
Laboratorio de Cristalografía Aplicada, Escuela de Ciencia y Tecnología, Universidad Nacional de San Martín (UNSAM), Campus Miguelete, 25 de Mayo y Francia, 1650 San Martín, Provincia Buenos Aires, Argentina

C. Escudero
ALBA Synchrotron Light Source, Carrer de la Llum 2-26, 08290 Cerdanyola del Vallès,

Barcelona, Spain

J. C. Hernández-Garrido, J. J. Calvino, M. López-Haro
Department of Material Science and Metallurgic Engineering and Inorganic Chemistry, Faculty of Science, University of Cádiz, Puerto Real (Cádiz), 11510 Spain

Keywords: *metal clusters, metal-like nobility, subnanometer-sized materials catalysis, reversible oxidation, quantum collective effects, collective charge transfer, wet-chemical synthesis*

Subnanometer-sized metal clusters often feature a molecule-like electronic structure, which makes their physical and chemical properties significantly different from those of nanoparticles and bulk material. Considering potential applications, there is a major concern about their thermal stability and susceptibility towards oxidation. Cu clusters of only 5 atoms (Cu_5 clusters) are first synthesized in high concentration using a new-generation wet chemical method. Next, it is shown that, contrary to what is currently assumed, Cu_5 clusters display nobility, beyond resistance to irreversible oxidation, at a broad range of temperatures and oxygen pressures. The outstanding nobility arises from an unusual reversible oxidation which is observed by in situ X-ray Absorption Spectroscopy and X-ray Photoelectron Spectroscopy on Cu_5 clusters deposited onto highly oriented pyrolitic graphite at different oxygen pressures and up to 773 K. This atypical property is explained by a theoretical approach combining different state-of-the-art first principles theories. It reveals the essential role of collective quantum effects in the physical mechanism responsible for the nobility of Cu_5 clusters, encompassing a structural 'breathing' through concerted Cu–Cu elongations/contractions upon O_2 uptake/release, and collective charge transfer as well. A predictive phase diagram of their reversible oxidation states is also delivered, agreeing with the experimental observations. The collective quantum effects responsible of the observed nobility are expected to be general in subanometer-sized metal clusters, pushing this new generation of materials to an upper level.

1 Introduction

Geometry and electronic structure of transition-metal nanoparticles change drastically when the size is reduced below 1−1.5 nm (i.e., below 100−150 atoms) due to quantum confinement effects.[1,2] When this size regime can be reached, the metal band structure is broken, and a series of discrete electronic levels are formed. This change gives rise to novel properties entirely different from those of bulk or larger nanomaterials.[3] In particular, when the cluster size is reduced to a very small number of atoms, a sub-nanometer network of molecule-like d orbitals centered on the metal atoms is formed, with the inter-atomic connections having the length of a chemical bond (1–2 Å). The special resulting structures make all the metal atoms cooperatively active in the given catalytic process, offering an excellent and economical employment of metal loading, which is relevant in applications.

Recently, subnanometer copper-based materials have attracted much interest in the field of catalysis.[4] This way, copper clusters have shown important catalytic properties e.g. for the oxidation of CO[5,6] and the reduction of CO_2,[7] the selective hydrogenation of olefin and carbonyl groups,[8,9] and in C-X (being X = C, N, S, P) bond forming reactions.[10] When these clusters are supported on titanium dioxide,[11] photon energy is temporarily stored in the form of charge pairs in the direct vicinity of the surface which is a prerequisite for follow-up chemistry.[7,12]) Moreover, it has been observed in many cases that these clusters are able to catalyze reactions at lower temperatures and pressures compared to bulk and conventional nanosized materials.[13] Yet, the inquiry is whether the well-known and undesired feature of an favourable, irreversible oxidation observed for Cu nanoparticles, which is assumed to become more likely as their size decreases, translates into the 'quantum' world of copper clusters consisting of just a few metal atoms.

Clusters of five Cu atoms (Cu_5 clusters) are synthesized in this study by a modified version of a previously reported electrochemical method,[14] allowing their production with the high concentrations necessary for applications in catalysis of industrial importance. These clusters show an exceptional chemical and thermodynamical stability in solution over the whole pH range.[14] Ex situ measurements[4] and theoretical studies considering the adsorption of one oxygen molecule[4,15,16] have provided some hints on their resistivity to irreversible oxidation at temperatures below 423 K. Up to date, however, the stability of Cu_5 clusters under laboratory conditions has remained an open question due to the absence of the necessary in situ experimentally-determined and quantitative characterization of such stability, and the need of a theoretical model capable of explaining the fundamental processes behind it.

To achieve conclusive evidence on the stability of Cu_5 clusters and the associated responsible mechanism, we conduct a quantitative investigation of well-characterized Cu_5 clusters. During exposure to controlled oxygen pressure and temperature, we identify the average oxidation states of Cu atoms in the cluster at each thermodynamic condition. We employ a combination of in situ X-ray Absorption Near Edge Spectroscopy (XANES) and Near-Ambient Pressure X-ray Photoelectron Spectroscopy (NAP-XPS) on Cu_5 clusters supported on Highly Oriented Pyrolytic Graphite (HOPG). The experimental setup allows a precise control of the O_2 loading and temperature to experimentally obtain a reversible mixture of different oxidation states for the Cu atoms composing the clusters at the different thermodynamic conditions. With the aim of explaining the experimental observations, a theoretical approach combining different methods of state-of-the-art first-principles theory is developed ad hoc. Such an approach not only allows to demonstrate that the experimentally observed reversible changes in the oxidation states of the Cu_5 clusters can be fully explained and quantitatively reproduced, but also enables to deliver fundamental understanding of the underlying mechanism.

Our study shows that Cu_5 clusters are not only capable of reversibly fixing a tunable proportion of neutral dioxygen (O_2) and charged superoxo (O_2^-) and peroxo (O_2^{2-}) species: they are also able of releasing them as neutral O_2 molecules upon increasing the temperature and decreasing the oxygen pressure, recovering thus their metallic phase, and behaving then as a noble metal. Contrary to what has been previously assumed,[4,15,16] the observed nobility of Cu_5 clusters goes far beyond their resistance to an irreversible oxidation due to quantum collective effects, encompassing concerted atomic nuclei motion and collective charge transfer as well. Besides securing the stability required for applications in industry, the discovered nobility opens a new avenue for the understanding and control of the catalytic activities of subnanometer-sized metal clusters, pushing this new generation of materials to an upper level.

2 Results and discussion

The synthesis of Cu_5 clusters was carried out by a modified version of a previously reported electrochemical method,[14] implying a step further the state-of-the-art in wet chemical synthesis of monodisperse clusters:[4,14] It allows the production of these clusters with the high concentrations that are necessary in spectroscopic XANES and NAP-XPS measurements (in the range $\approx$ 40 mg/L and efficiencies near 70%, for details see Methods Section) and, more generally, their application in catalysis.

Figure 1a shows the emission spectrum (excitation at 224 nm) of a cluster sample. It can

be observed the presence of just one emission peak (305 nm = 4.07 eV) indicating a large degree of monodispersity of clusters samples, similar to those previously produced with much lower concentration.[14] The estimated size from the Jellium model, which seems to be good approximation for clusters without strong binding ligands, is $N=(E_F/E_g)^3 \approx 5$ (being E_F the Cu Fermi level = 7.0 eV, and E_g the HOMO-LUMO gap ≈ emission peak). Figure 1b–c shows the results of an Aberration-Corrected Scanning Transmission Electron Microscopy study, working in the High Angle Annular Dark Field imaging mode (AC-STEM-HAADF), of the synthesized clusters at very low concentration (≈ 10 ng/mL, corresponding to less than ≈ 1 monolayer) compared with that employed for further experimental characterization using X-ray spectroscopy. The visualization of the Cu_5 clusters has been improved by submitting raw images to an advanced image processing which included denoising and background subtraction (see Supplementary Figure 1). To determine, in a fully automated, user-independent and statistically meaningful way, the size of the clusters observed in the experimental images, a segmentation based on k-means clustering techniques was performed (see Figure 1b, Supplementary Figure 2a-c and Methods Section for details). To validate this analysis, HAADF-STEM images were calculated for models of Cu_3 and Cu_5 clusters, in the last case considering both planar (2D) and trigonal bipyramidal (3D) structures (see Supplementary Figure 2d). Then, the histogram and cumulative histogram from five different experimental HAADF-STEM binarized images were calculated (Figure 1c). The analysis indicates that about 85% of the Cu clusters in this sample are below 0.5 nm in size. According to the luminescence results, the remaining part of the distribution, with size in the range 0.5 - 0.9 nm, should correspond to the superposition of neighboring clusters in the same area. Specifically, the diameter histogram (see left panel of Figure 1c) shows a narrow size distribution with a mean cluster size about 0.40 ± 0.03 nm, a value agreeing very well with the expected value for the 3D Cu_5 clusters. This estimation of the clusters size is close to that previously reported for similar samples.[1] A small proportion (≈ < 10-15%) of smaller Cu_3 clusters (not detected in the luminescence spectra) could also be present in the samples.

2.1 In situ XANES and NAP-XPS experiments:

To investigate the stability of Cu_5 clusters in presence of oxygen molecules, we performed X-ray Absorption Near Edge Structure Spectroscopy (XANES) experiments at the Cu K-edge in air, at different temperatures. Cu_5 clusters were deposited on HOPG, which exhibits a weak interaction with the clusters.[4] According to an experimental estimation by XPS, considering the intensity of C 1s and Cu 2p photopeaks (see Supplementary Figure 3), the final concentration in the sample represents about 10 monolayers of Cu_5 clusters on the HOPG surface. Figure 2a shows the XANES spectra at Cu K-edge absorption of the Cu_5 cluster on HOPG collected while heating up from room temperature (RT) to 523 K and cooling down back to RT after removing the hydration shell from the mother's solution (see Supplementary Figure 4 and 5). All spectra exhibit the characteristics associated to Cu(II), that are, the energy edge located at 8986 eV and the weak feature (pre-peak) at 8977 eV. When the sample is cooled down at RT, no changes in the XANES spectra are observed, indicating that the Cu clusters remain dehydrated and without any other apparent structural changes (spectrum at the bottom in Figure 2a).

Then, when temperature is increased above 573 K, Cu_5 clusters lose their stability (Figure 2b). Indeed, XANES spectrum show drastic changes at 673 K, with no modifications after cooling, confirming an irreversible transformation. The final XANES spectrum obtained

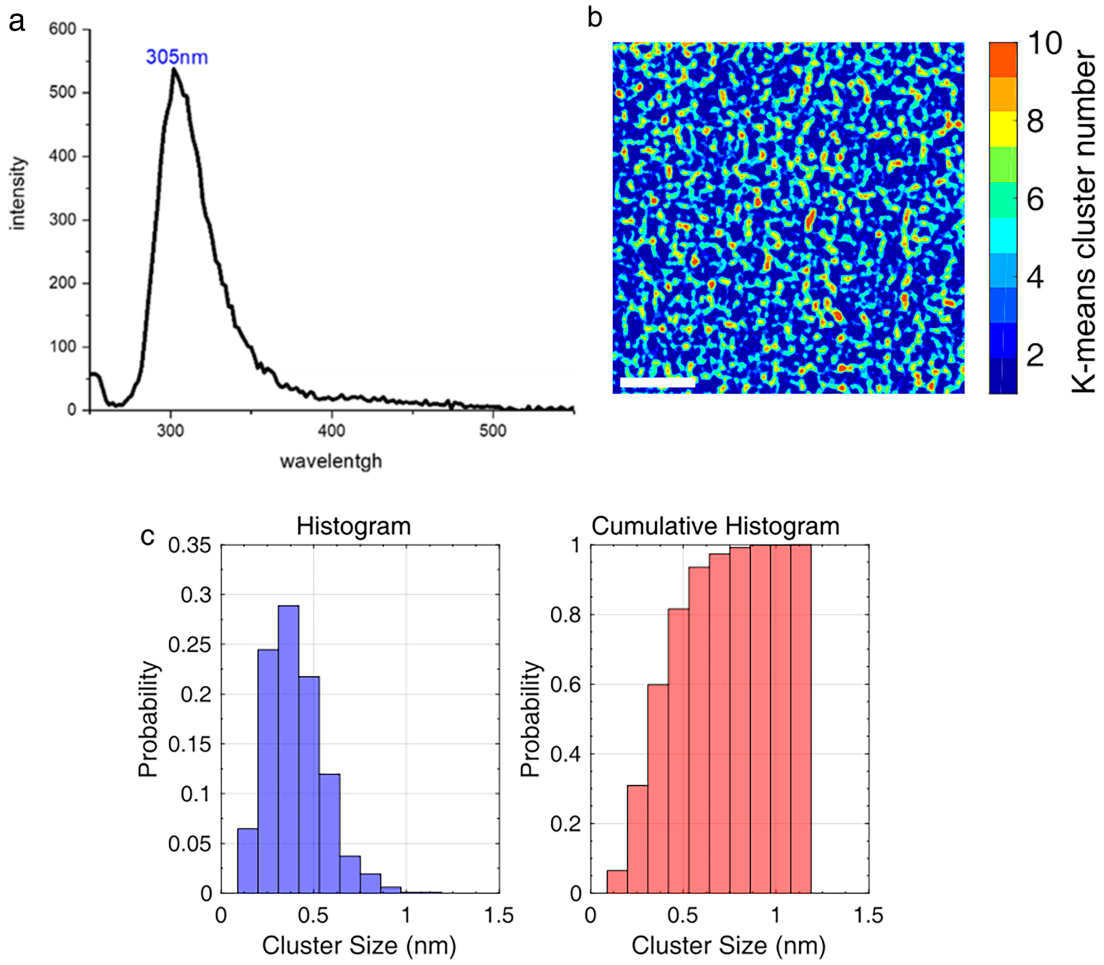

Figure 1. Characterization of the synthesized Cu clusters. a) Emission spectrum of a cluster sample (excitation at $\lambda = 224$ nm) of the synthesized Cu clusters; b) k-means clustering result from experimental AC-STEM-HAADF image; c) Clusters size distribution histogram obtained after clustering and segmentation. The statistical analysis shows that about 85% of the Cu clusters in this sample are below 0.5 nm in size. The error bar derives from estimating the average cluster size after eroding (-) and dilating (+) by 1 pixel each object in the whole set of binarized images.

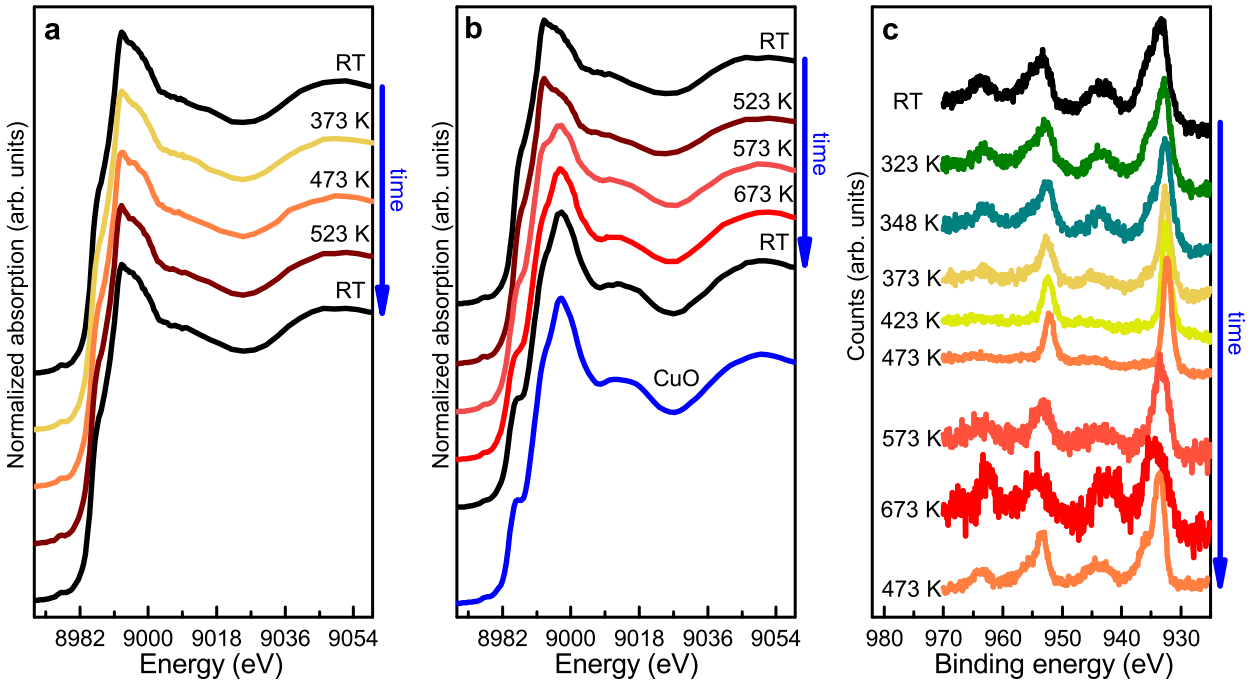

Figure 2. a) XANES spectra at the Cu K-edge of Cu_5 clusters supported on HOPG after removing the hydration shell from the mother solution, collected in air from RT to 523 K and back to RT showing no changes at the clusters; b) XANES spectra at the Cu K-edge of Cu_5 clusters supported on HOPG collected in air from RT up to 673 K and back to room temperature, showing the formation of bulk CuO. The spectrum of CuO (blue) is shown as a reference; c) Cu $2p$ XPS spectra of Cu_5 clusters on HOPG collected with a photon energy of 1350 eV at 0.15 mbar of oxygen from RT to 673 K and back to 473 K. A reduced state for Cu is only present in the 373−473 K range.

corresponds to that of bulk CuO (Figure 2b), indicating a fusion of the Cu_5 clusters. This effect leads to the formation of bigger copper domains which are oxidized to CuO, resembling the behavior of Cu nanoparticles. Thus, we can conclude that the initial state of the Cu atoms on the supported clusters, under atmospheric conditions at RT, corresponds mainly to the Cu(II) oxidation state. Remarkably, at atmospheric pressure, the Cu_5 clusters are structurally and chemically stable up to 523 K. Above this temperature, the Cu_5 clusters, deposited at high density on HOPG substrate, fuse and leads to the irreversible formation of bulk CuO.

In order to determine the influence of the oxygen pressure on the stability of Cu_5 clusters against an irreversible oxidation process, an additional NAP-XPS experiment was performed. Different oxygen pressures were examined to determine the most suitable for these experiments (see Supplementary Figure 7). XPS allows a qualitative identification of Cu(0), Cu(I) and Cu(II) oxidation states. Cu(II) has a distinctive collection of broad satellite features at 943 eV and 963 eV. Additionally, Cu $2p_{3/2}$ and Cu $2p_{1/2}$ photopeaks become shifted by 0.5 eV, and are significantly broader than those of Cu(I) and Cu(0). The Cu(I) state can be differentiated from metallic Cu by only a satellite peak at 945 eV.

Figure 2c shows the Cu $2p$ photoemission peaks of the Cu_5 cluster supported on HOPG, at the same concentration used for Cu K-edge XANES experiments, but measured at 0.15 mbar of oxygen from RT to 673 K. Below 373 K the shape of the photopeaks and the appearance of the satellites peaks indicate that the main state of Cu atoms is Cu(II). An unexpected behavior was observed during the thermal treatment between 373 and 473 K, because a drastic reduction of the Cu atoms oxidation state occurred under this O_2 pressure, indicated by the narrowing of the photoemission peaks and the disappearance of the satellites peaks. A similar behavior was observed at high vacuum (HV) (see Supplementary Figure 8). Cu atoms with Cu(II) oxidation state are not observed above 423 K as they are reduced. Above 573 K, photoemission peaks became broader and satellites reappeared indicating that the oxidation state of Cu atoms in the clusters is Cu(II) again. The reduced oxidation state of Cu atoms was never recovered after heating at 673 K, as it is demonstrated in the final XPS spectrum taken at 473 K at the end of the treatment, which shows the presence of Cu(II) mainly (lowest spectrum in Figure 2c). This result is consistent with an irreversible oxidation of the sample, as in the XANES Cu K-edge experiments, when the sample was heated up to 673 K at atmospheric pressure. In general, above a threshold temperature of 573−673 K, the Cu atoms in the clusters oxidize irreversibly to Cu(II) in the presence of O_2, presumably to form CuO. A similar experiment in HV pressure of 1.5×10^{-7} mbar, showed the formation of bulk metallic Cu after heating up to 673 K (see Supplementary Figure 6). In summary, both XANES and NAP-XPS experiments performed at low or high pressures of oxygen, indicate the fusion of clusters forming bulk phases at temperatures above 573 K.

XANES spectroscopy at the Cu L_3-edge is a proper technique for quantitative measurements of copper oxide mixtures. CuO and Cu_2O have strong absorption edges at 931.3 eV (peak 1, P1 in Figure 3) and 933.7 eV (peak 2, P2 in Figure 3), respectively, and substantial shape differences between them and that corresponding to metallic Cu, allowing an easy identification of each oxidation state (see Supplementary Figure 9). Thus, the Cu L_3-edge XANES spectra of those reference compounds can be used as reliable fingerprints to identify the different oxidation states and their relative concentration in the sample for different thermodynamic equilibrium conditions. Figure 3 shows the in situ Cu L_3-edge XANES spectra of Cu_5 clusters on HOPG.

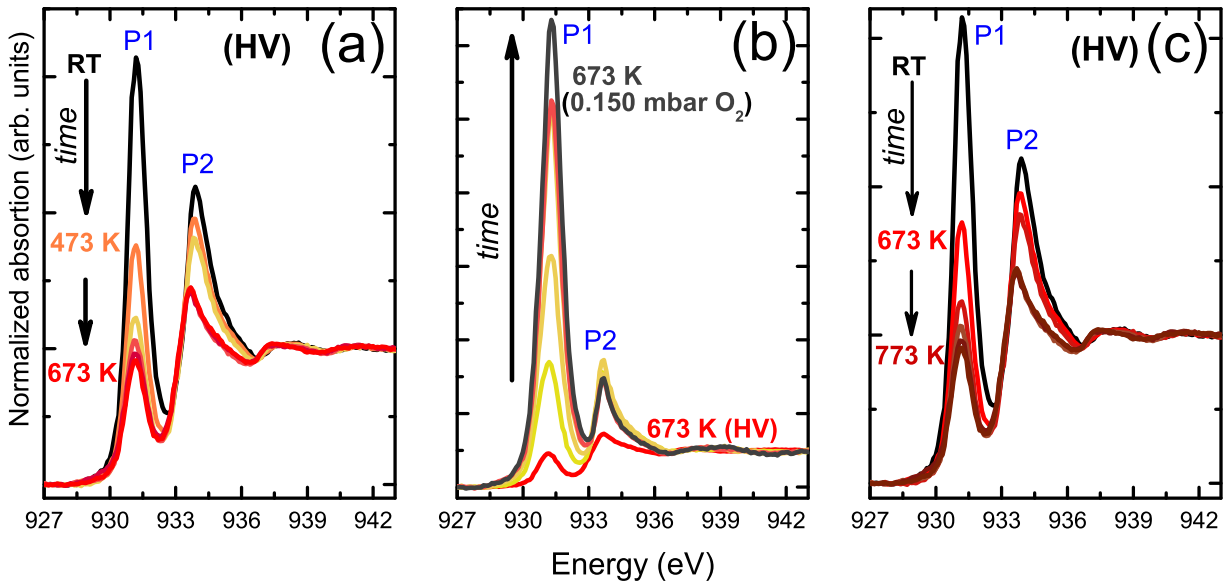

Figure 3. Cu L_3-edge XANES spectra collected in situ of Cu_5 clusters on HOPG. a) *Stage 1*: sample preparation obtained at HV during degassing of oxygen by heating; b) *Stage 2*: oxidation in presence of 0.15 mbar of oxygen background pressure at 673 K; c) *Stage 3*: reduction at HV during heating in vacuum of Cu_5 clusters on HOPG after oxidation (*Stage 2*).

Before the oxygen dosage to the experimental main-chamber, the sample was heated up to 673 K at HV conditions for hydration shell and oxygen removal. During this treatment (Stage 1) a pronounced decrease of the P1 signal with the simultaneous increase of P2 one was observed (see Figure 3a), not detecting the formation of bulk metallic Cu (see Supplementary Figure 9). After degassing, 0.15 mbar of oxygen was introduced in the chamber while keeping the temperature at 673 K (see Figure 3b, Stage 2). At this stage, the intensity of the P1 signal of the initial state of Stage 1 is recovered and even overcome. This strong increment is accompanied with the decrease of the P2 intensity. Finally, after reaching the equilibrium, the oxygen leak valve was closed and the sample was cooled down to RT. After reaching that temperature, the sample was heated up to 773 K in HV (see Figure 3c, Stage 3).

A linear combination fitting analysis of the Cu L_3-edge XANES spectra was performed in order to quantify the percentage of the Cu species with different oxidation states. The spectra of metallic Cu, CuO and Cu_2O were used as standards for the different oxidation states following the procedure described by Eren et al.[17] (see Supplementary Figure 10). Supplementary Figure 11 shows the percentage of copper oxidation states of Cu_5 clusters on HOPG as a function of temperature and O_2 pressure. The initial percentages of Cu species are recovered after the complete cycle. The qualitative behavior observed by Cu K-edge XANES and NAP-XPS, at atmospheric pressure and at 0.15 mbar of oxygen, are now confirmed and quantified by Cu L_3-edge XANES experiments up to higher temperatures (at least 773 K instead of 523 K). By decreasing the Cu_5 clusters percentage on HOPG we demonstrate that they are stable against irreversible oxidation, at least, up to 773 K, even at oxidizing conditions of 0.15 mbar of oxygen.

In order to get further insight into the reversible/irreversible oxidation of Cu_5 clusters, additional in situ Cu L3 -edge XANES measurements were performed at oxygen pressure of 0.15 mbar and different temperatures (see Supplementary Figure 11). It is interesting to

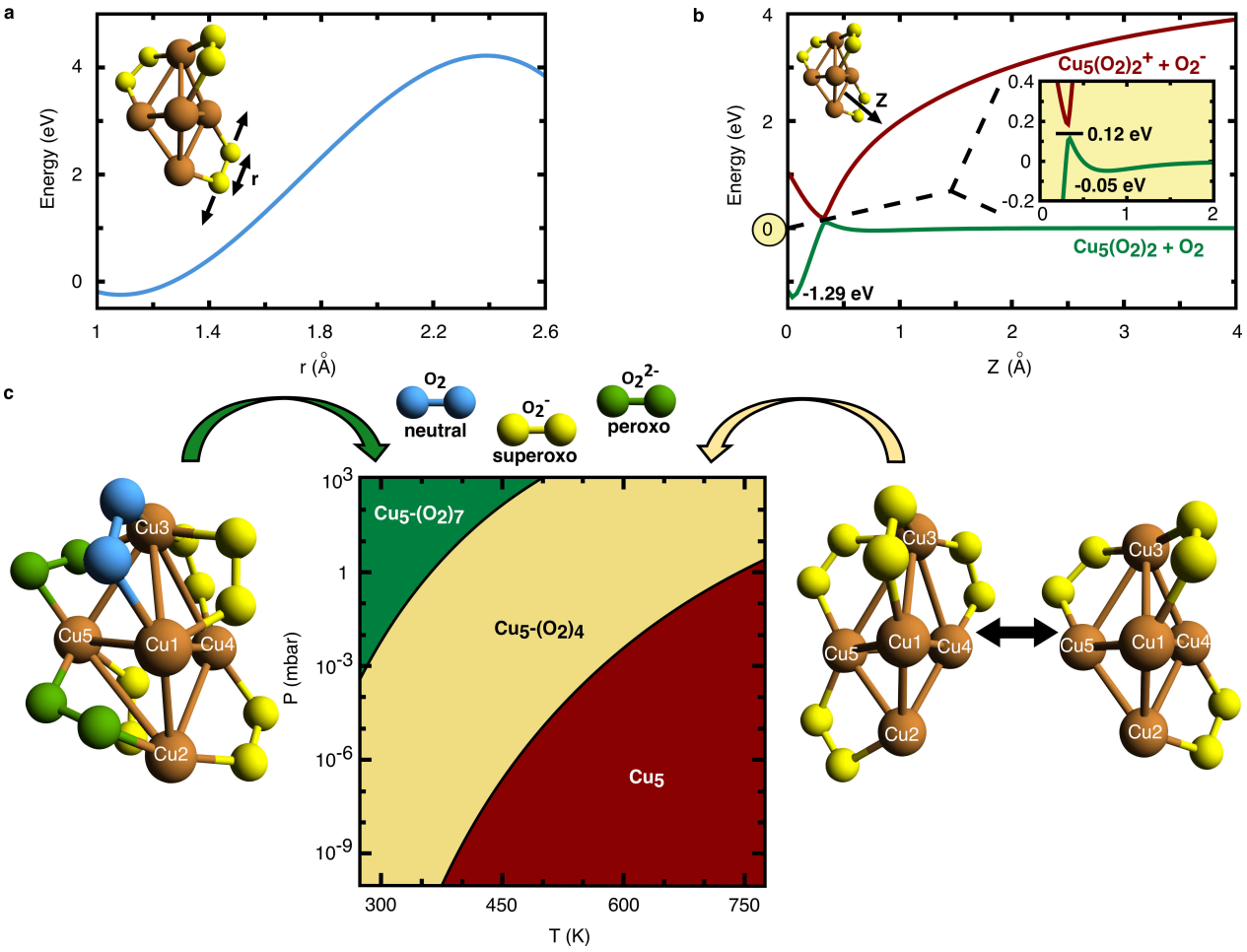

Figure 4. Theoretical characterization of Cu_5–$(O_2)_n$ complexes. a) Interaction energy as a function of the O–O distance r of one adsorbed O_2 molecule of the Cu_5–$(O_2)_3$ complex; b) O_2–$(Cu_5(O_2)_2)$ reaction energy pathway in the adiabatic ground (green) and excited (red) electronic states. The O–O bond length r has been optimized at each O_2–$(Cu_5(O_2)_2)$ distance Z; c) Phase diagram, showing the most probable Cu_5–$(O_2)_n$ complexes at each variable pair (p, T). Their optimized structures are also presented (at $T = 0$ K).

observe that there is an increase of the Cu(0) proportion - and a corresponding decrease of the oxidated form Cu(I) - when the temperature is increased from 293 to 423 K. The results confirm that, contrary to what is currently assumed, the oxidation state is reversed - in the presence of molecular oxygen - upon increasing the temperature, pointing out that some reversible mechanisms (as the oxygen molecular adsorption/desorption which we will describe below) should be involved in the observed reversibility of the copper cluster oxidation states.

2.2 Theoretical modelling: reversible molecular oxidation

According to the experimental results, and to be able of explaining the observed reversible oxidation of Cu_5 clusters, we assume that Cu_5 clusters can form a complex with (several) adsorbed O_2 molecules. In this way, the experimentally determined relative concentration of oxidation states (Supplementary Figure 11) can be reproduced theoretically by calculating the number of O_2 molecules that can be adsorbed depending on the oxygen pressure and temperature (Figure 5).

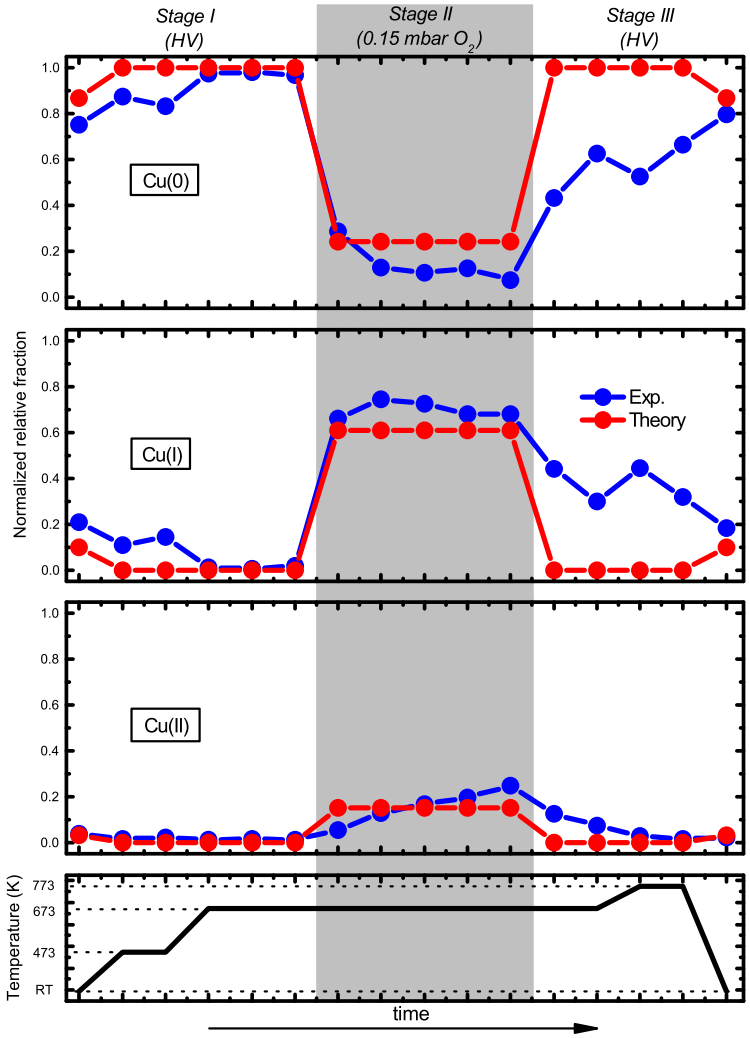

Figure 5. Comparison between theoretically and experimentally determined fractions of Cu(0), Cu(I) and Cu(II) oxidation states at high-vacuum (HV), oxygen pressure of 0.15 mbar and HV after treatment at 0.15 mbar of oxygen (stages I, II and III respectively). Theoretical values are determined through a Boltzmann-weighted average of the Helmholtz free energies for each complex and their associated distributions of oxidation states (see Supplementary Section 2.3). Error bars of experimental points are not shown for simplicity (see Supplementary Figure 11). The time axis is only indicative of the experimental sequence for each condition. Each experimental point was acquired after reaching thermodynamic equilibrium conditions. The acquisition time for each experimental point was about 15 minutes.

By adopting a multi-step and multi-scale approach, we first apply ab initio multi-reference theory considering the illustrative case of a single O_2 molecule interacting with the $(Cu_5(O_2)_2)$–O_2 complex. The application of multi-reference theory is necessary due to the multi-configurational nature of the wave-functions at the barriers between neutral and ionic electronic states. Methods using a common set of orbitals would require very large active size to describe both states correctly and thus would be prohibitively expensive due to the size of the system. Following the same strategy presented in Refs.[18,19] for molecular oxidation processes in extended systems (see Supplementary Section 9), the orbitals are first optimized using the single-state multi-configurational self-consistent-field (CASSCF) method separately for the electronic states correlating with neutral and ionic fragments (see Figure 4). Next, multireference perturbation theory is applied to account for dynamical correlation effects. Considering the general case of Cu_5–$(O_2)_n$ complexes, the O−O bond breaking is the rate-determining step for an irreversible oxidation. As illustrated in Figure 4a (see also Supplementary Figure 13 and 14) for the $(Cu_5(O_2)_2)$–O_2 interacting pair, the energy required to dissociate a chemisorbed molecule is very high (> 4 eV). Thus, although the formation of reaction products involving dissociated O_2 molecules can be thermodynamically favorable, it is kinetically forbidden at the experimental temperature range from RT up to 773 K. On the contrary, the barriers from physisorption to molecular chemisorption states are low (ca. 0.1 eV), favoring the formation of molecular chemisorption products. This is illustrated in Figure 4b and Supplementary Figure 13 and 14. As shown in Figure 4b, the asymptotic limit correlating with ionic fragments is so high that the charge, originally donated to the O_2 species at the molecular chemisorption state, is transferred back to the cluster to allow the desorption of the neutral O_2 molecule, rendering the oxidation reversible. Therefore, the application of multireference theory shows (1) high energy barriers for O−O bond breaking, hindering an irreversible oxidation, and (2) low energy barriers from physisorption to chemisorption states, favoring reversible molecular oxidation processes upon successive steps of attachment/release of O_2 molecules.

Once it has been demonstrated that O_2 adsorbs to Cu_5 clusters in molecular form, dispersion-corrected DFT is employed to obtain optimized geometries of large molecular Cu_5–$(O_2)_n$ complexes ($n \leq 10$). The structural optimizations are carried out using the Perdew-Burke-Ernzerhof (PBE) density functional[20] and the Becke-Johnson (BJ) damping[21] for the D3 dispersion correction. The optimized Cu_5–$(O_2)_n$ structures (Figure 4c and Supplementary Figure 15) show enhanced stability (see Supplementary Figure 16) when the O_2 molecules attach to bridge Cu_5 positions. Depending on their number, the O_2 molecules can be absorbed as neutral (O_2), superoxo (O_2^-), or peroxo (O_2^{2-}) species. Since dispersion forces allow a stretching of the Cu–Cu distances, the Cu_5 can adapt its shape to accommodate the charged O_2 species, featuring larger O−O bonds, at its bridge sites (see Supplementary Figure 17).

The adsorption of (up to 7 mostly charged) O_2 molecules on Cu_5 clusters is the result of collective motions of electrons and atomic nuclei. A "breathing" effect due to concerted elongations/contractions of the Cu−Cu bonds enables the adsorption/release of O_2 molecules (see Supplementary Figure 18). As shown in the same figure, the negative charge is collectively donated from the $3d$ orbitals of the copper atoms and shared by the π^* orbitals of several O_2 molecules. The charge donation from one copper atom to one O_2 molecule activates a reorganization of the subnanometer-sized network formed by the $3d$ orbitals of all copper atoms, making a collective charge donation possible, also illustrated in Supplementary Figure 18

and 19. A collective back-donation transfer process from s-type orbitals of the adsorbed O_2 molecules to p-type orbitals of the copper atoms has been also identified (see Supplementary Figure 20). The collective adsorption process thus leads to the migration of electron charge from the copper clusters to the adsorbed O_2 molecules on its surface but not to the rupture of Cu-Cu and O-O chemical bonds, making possible that the clusters recover their metallic phase upon O_2 release by heating or decreasing the oxygen pressure, as experimentally observed and quantitatively reproduced by theory, as we will describe below.

2.3 Theoretical phase diagram of Cu_5–$(O_2)_n$ complexes and comparison to experiment:

At a given temperature (T) and partial oxygen pressure (p), we have determined the relative stability of complexes Cu_5–$(O_2)_n$ by calculating their Helmholtz free energies of formation,[22,23,24,25]

$$\Delta F_f(p,T) = F_{Cu_5-(O_2)_n}(T) - F_{Cu_5}(T) - n \cdot \mu_{O_2}(p,T) \quad (1)$$

where $F_{Cu_5-(O_2)_n}$ and F_{Cu_5} are the Helmholtz free energies of the Cu_5–$(O_2)_n$ complex and the bare Cu_5 cluster, respectively. The dependence on O_2 pressure is introduced via μ_{O_2}, the chemical potential of molecular oxygen. For an easier interpretation, this expression is written in terms of the thermodynamical potential ω[22] defined as:

$$\omega(T,\mu_{O_2},n) = \Delta E_{F,\mathrm{corr}}(T) - T \cdot s_{Cu_5-(O_2)_n}(T) + T \cdot s_{Cu_5}(T) - n \cdot \mu_{O_2}(p,T). \quad (2)$$

In a first approximation (see Supplementary Section 14 for details), the Cu_5 clusters are treated as fully immobilized on the support and are coupled to a heat bath of temperature T and an infinite reservoir of O_2 gas at pressure p. Under these idealized conditions, the ω potential will become minimal at thermodynamic equilibrium. From this expression, the number n of adsorbed O_2 molecules which minimizes ω for a specified temperature and a given oxygen pressure can be obtained as follows: $\Delta E_{F,\mathrm{corr}}$, the first term on the right-hand side of Eq. 2, corresponds to the formation energy of Cu_5–$(O_2)_n$ and is defined as

$$\Delta E_{F,\mathrm{corr}}(T) = E_{Cu_5-(O_2)_n} - E_{Cu_5} - n \cdot E_{O_2} + E_{\mathrm{corr}}(T), \quad (3)$$

where $E_{Cu_5-(O_2)_n}$ and E_{Cu_5} denote the DFT energies of the oxygen-covered and pure cluster, respectively, and E_{O_2} is the DFT energy of molecular oxygen. E_{corr} is introduced to account for the zero-point energy, the thermal vibrational contribution as well as thermal rotational, and translational terms. The next term on the right-hand side of Eq. 2 introduces a correction with respect to the entropy $s_{Cu_5-(O_2)_n}$ of the cluster. Assuming immobilized copper particles, only vibrational and electronic excitation or degeneracies can contribute to the entropy. The (p,T)-phase diagram is then created by determining the number n of adsorbed O_2 molecules which minimizes ω (or ΔF_f) for a specified temperature and a given oxygen pressure (see Figure 4c, Supplementary Figure 21 and 22). Measurable oxidation states [Cu(0), Cu(I), Cu(II)] can be assigned to each copper atoms for a given Cu_5–$(O_2)_n$ complex (see, e.g., Supplementary Figure 15 and 20). To fully account for the thermodynamical conditions, a Boltzmann-weighted average of their Helmholtz free energies and associated distributions of oxidation states is carried out for each variable pair (p,T) (see Figure 5 and Supplementary Table 2).

At RT and atmospheric pressure, the Cu_5–$(O_2)_7$ complex stands by as the most stable, with $\Delta F_f < -5$ eV (see Supplementary Figure 21). All oxygen molecules become adsorbed

at bridge sites of the Cu_5 clusters as neutral (O_2), superoxo (O_2^{-1}), or peroxo (O_2^{-2}) species, with most of the copper atoms bearing the Cu(II) oxidation state. Accordingly, only the Cu(II) state is inferred from the XANES measurements of Cu_5 clusters taken at atmospheric pressure and the same spectra are recorded from RT up to 523 K (see Figure 2). In fact, as can be seen in Figure 4c, the phase of the Cu_5–$(O_2)_7$ complex (shown in red) persists up to about 500 K at atmospheric pressure. The analysis of the wavefunction obtained using multi-reference theory for the Cu_5–$(O_2)_7$ complex (see Supplementary Figure 20) reveals a spin density close to unity for most Cu atoms, a clear signature of Cu(II) oxidation states.

At atmospheric pressure, upon heating to ca. 500 K, the Cu_5–$(O_2)_7$ complex loses O_2 molecules and the Cu_5–$(O_2)_4$ and Cu_5–$(O_2)_3$ complexes become the most stable, with a free energy of about −4 eV (see Supplementary Figure 21). When the pressure is lowered to ca. 0.15 mbar at 350 K, the Cu_5–$(O_2)_4$ complex is the most stable (see Figure 4c), being quasi-iso-energetic with the Cu_5–$(O_2)_3$ complex (see Supplementary Figure 21). The analysis of the wave-function obtained using multi-reference theory confirms that the Cu_5 clusters become carriers of superoxo O_2^- radicals (with a spin very close to unity), with most of the copper atoms assigned to the Cu(I) oxidation state (see Supplementary Section 13.1 and Figure 19). These complexes are still stable upon heating to 673 K, explaining why the experiment shows that the Cu(I) oxidation state is dominant (see Figure 2). Further lowering of the oxygen pressure from 0.15 mbar to HV at a constant temperature of 673 K makes the copper cluster lose all O_2 molecules so that the bare Cu_5 cluster appear in the phase diagram as the predominant species (red area in Figure 4c). This outcome clearly signals the occurrence of a reversible molecular oxidation, with the Cu_5 clusters recovering the donated charge upon O_2 desorption. Consequently, the Cu(0) oxidation state becomes the major component, as experimentally shown at HV and 673 K (Figures 3 and 5).

Reactivity is expected to be under kinetic control at RT and HV and the O_2 molecules can become trapped at the physisorption minimum since there is a low, yet noticeable barrier between physisorption and molecular chemisorption states (ca. 0.1 eV, see Figure 4b). Once the probability of trapping at the physisorption state is considered (see Supplementary Section 15), the theoretical model predicts the Cu(0) oxidation state to be dominant (see Figure 5 and Supplementary Figure 23). By including non-adiabatic effects via the Landau-Zener model[26,27,28] (see Supplementary Section 15), very close values of the fractions of the oxidation states are obtained. At thermodynamic equilibrium, using the Boltzmann-weighted average of the free energies for all complexes in their corresponding oxidation states, we reach a clear quantitative agreement with the experimentally determined fractions at 0.15 mbar (see Figure 5 and Supplementary Figure 23) as well.

3 Conclusion

Bare Cu clusters of five atoms, synthesized by an improved electrochemical method, show an outstanding stability against oxidation at least up to 773 K at 0.15 mbar of oxygen pressure. High energy O_2 dissociation barriers prevent the formation of reaction products involving dissociated O_2 molecules, and then an irreversible oxidation, in the experimental energy range. Instead, Cu_5 clusters display a reversible O_2 adsorption behavior, circling through different oxidation states of Cu atoms at varying temperature and oxygen pressure. As demonstrated by applying multireference ab initio theory, this noble-like behaviour is favored due to both the low values of the energetic barriers (ca. 0.1 eV) from physisorption

to molecular O_2 chemisorption states as well as the high O_2 dissociation energy barriers (> 4 eV). Combining dispersion-corrected DFT theory with first principles thermochemistry, a phase diagram of Cu_5–$(O_2)_n$ complexes ($n \leq 10$) is created, matching the experimental observations performed during reaction conditions. The reversible adsorption of O_2 is the result of concerted rearrangements of the atomic nuclei and coordinated charge transfer processes within a network of Cu $3d$ orbitals.

This work demonstrates that Cu_5 clusters form complexes with the adsorbed O_2 molecules, Cu_5–$(O_2)_n$, with the positive charge being located on the Cu atoms, and the corresponding negative charge on the attached O_2 molecules. This charge transfer only exists in the complex and when the O_2 molecules desorb, the copper atoms remain unoxidized. Thus, the Cu_5 clusters cannot exist oxidized as an independent species. They can present several oxidation states while O_2 molecules are absorbed, but recover their metallic phase upon gas release, thus behaving as a noble metal. Our findings changes our current understanding of the fundamental mechanisms driving clusters oxidation/reduction processes, paving the way for a better comprehension and control of their catalytic activities. Thus, the outstanding nobility displayed by Cu_5 clusters warrants the stability necessary in industrial technological applications. The discovered collective mechanism has its origin in the sub-nanometer size of the actual quantum system and is therefore fundamentally different from that occurring in larger clusters on the nanoscale or bulk materials. In particular, it is clear that the collective quantum mechanism responsible of the observed nobility is not specific of the Cu_5 cluster and the same behaviour can be expected for any cluster size in which concerted motions of inter-connected atoms become possible. This study thus illustrates the great potential that lies in this new class of materials, offering a new paradigm at subnanometer science.

4 Methods Section

Materials and methods:
Copper clusters were obtained by using an electrochemical method with an Autolab PGSTAT 20 potentiostat. A Methrom thermostated-3 electrode electrochemical cell was employed, with a copper sheet of 10 cm^2 as the working electrode, a platinum sheet of 10 cm^2 as the counter electrode, and a hydrogen electrode as the reference. The working and counter electrodes were placed vertically face to face at a distance of 1.5 cm. Pure MilliQ water (conductivity $\approx 6.26\ \mu\ \Omega/cm^3$) without any added electrolyte was used, and N_2 was bubbled during 30 min in order to deareate the solution. The synthesis was carried out at constant temperature (298 K) at a constant Voltage of 1V for 1500 s. The Cu sheets were carefully cleaned before the synthesis: it was first polished with sand paper (600 grid) followed by aluminia ($\approx$ 50 nm), washed out thoroughly with MilliQ water and sonicated. After the synthesis, the remaining Cu^{2+} ions were precipitated by NaOH (pH $\approx$ 12), subsequent filtration, and finally the pH was adjusted to 7 by addition of $HClO_4$. A typical concentration of clusters obtained after purification is in the range $\approx$ 40 mg/L. The typical yield of cluster synthesis, taking into account the difference between Cu content obtained by flame atomic absorption spectroscopy and the Cu^{2+} content obtained by ion selective electrode, is around 70%.

HOPG supported Cu_5 clusters were prepared by a simple dripping method. Water solution containing approximately 100 mg/L (i.e., 100 μg/mL) of Cu_5 clusters was dropped onto highly oriented pyrolytic graphite (NT-MDT ZYB 10 x 10 x 2.0 mm) avoiding the contact of

the solution with the HOPG borders. HOPG was previously cleaned by several mechanical exfoliations using the sticky tape method. After deposition the HOPG surface was cleaned with MilliQ water in order to obtain a thin layer of Cu_5 clusters and remove other impurities. The sample was then dried in air at 343 K during 1 hour.

Samples for electron microscopy studies were prepared by depositing one drop of the synthesized clusters solution (1:10000 diluted, i.e., with a cluster concentration $\approx$ 10 ng/mL, which would correspond to less than 1 monolayer of clusters) onto holey-carbon coated Au grids. After their preparation, the TEM samples were conserved under vacuum conditions. Scanning-Transmission Electron Microscopy studies, using High-Angle Annular Dark-Field, HAADF-STEM, which contrasts are related to the roughly Z^2 atomic number of the elements under the beam, were performed on a FEI Titan Themis 60–300 Double Aberration Corrected microscope operated at 200 kV. We corrected the aberrations of the condenser lenses up to fourth-order, using the Zemlin tableau to obtain a sub-Angstrom electron probe. A condenser aperture of 50 μm yielding an electron probe with a convergence angle of 20 mrad was used. To limit the damage by the electron beam, a fast image recording protocol was used by combining a beam current of 25 pA, a 2.5 μs dwell time and an automated fine-tuning alignment of A1 and C1 using the OptiSTEM software. To obtain images with good quality, the beam current and image acquisition time should be optimized according to the stability of the sample under the beam.

Aimed to quantitatively characterize the Cu clusters, a specific methodology for the digital analysis of the experimental images has been developed and coded in a home-made MATLAB script. First, to improve the signal-to-noise, the AC HAADF-STEM images were denoised by combining the Anscombe variance stabilization transform (Anscombe VST) with the Undecimated Wavelet Transform (UWT). The background from the denoised images was subtracted by disk top-hat filtering, allowing us to improve the visibility of the ultrasmall clusters.

To determine in a fully automated, user-independent and statistically meaningful way the size of the clusters observed in the experimental images, a segmentation based on k-means clustering techniques was performed, a methodology fully described in Liu et al.[29] k-means clustering is an unsupervised machine-learning algorithm, which classifies and splits a dataset into groups (clusters) with certain similarities. Thus, in the case of microscopy images, this algorithm will group and classify pixels with similar intensities into a fixed number of clusters (k). This total number of clusters, k, is usually chosen on the basis of previous experience in the analysis of similar problems. Note that, a k cluster number about 10 was found as the optimum value for our HAADF-STEM images. It is important to mention that, after using this algorithm, the image will be transformed into an array of classified datasets. In our case, each pixel will be included only in one of the 10 clusters, i.e. in a specific cluster number. This allow us to separate the different features that form the image by appropriately selecting specific values, or range of values, of the cluster numbers. Once such constrain is made, the image is transformed into a binarized image in which the pixels corresponding to the selected number of clusters are set to 1, whereas the rest are set to 0. To validate the k-means analysis and confirm our clusters detection and segmentation procedure, HAADF-STEM images were calculated for modelled Cu_3 and Cu_5 clusters, in the last case considering both planar (2D) and trigonal bipyramidal (3D) structures (Supplementary Figure 2d) using the electron-optical parameters from the experimental STEM studies: HT = 200 kV, Cs3 = 0.001 mm, Cs5 = 5 mm, df = 30 Å and HAADF detector angle collection = 49 to 200 mrad.

The HAADF-STEM image simulation was carried out using TEMSIM software.[30] The Cu clusters models used as input in these simulations were built using the Rhodius software developed at UCA.[31] The k-mean cluster analysis was carried out for each calculated image, using a k cluster number equal to 10 and binarization by selecting cluster numbers from 8 to 10 (Supplementary Figure 2d middle and right-hand side). As before, the orange object corresponds to the Cu clusters and the blue area is associated to the background. Note how, the k-means clusters analysis indicates that the pixels corresponding to the clusters from 8 to 10 can appropriately account for the projected area of the Cu clusters in the simulated image. The Cu cluster sizes was then estimated as the diameter of the circle with that area (equivalent diameter). The values of this diameter for the models were estimated as 0.38 nm for Cu_3 and as 0.56 and 0.41 nm for Cu_5 2D and Cu_5 3D clusters, respectively. Moreover, using this parameter, the histogram and cumulative histogram from five different experimental HAADF-STEM binarized images were calculated (Figure 1c and Supplementary Figure 2).

The detected objects with diameter in the 0.21 - 0.36 nm range must correspond to smaller Cu clusters. The remaining part of the distribution, with size in the range 0.5 - 0.9 nm, should correspond to the superposition of neighbouring clusters in the same area (see other characterization techniques). In any case, note how, the cumulative histogram indicates that about 85% of the Cu clusters in this sample are below 0.5 nm in size. From this one can conclude that the main cluster in the dispersion is Cu_5 with a small proportion of Cu_3 ($\approx <$ 10-15%).

X-ray Absorption Spectroscopy measurements (XAS) in the XANES (X-ray Absorption Near Edge Structure) region at the Cu K edge were performed at the XAFS2 beamline[32] of the Laboratório Nacional de Luz Síncrotron (LNLS), Campinas, Brazil. The measurements were performed in fluorescence mode using a Si(111) crystal monochromator around the Cu K-edge (8979 eV) in the energy range from 8900 to 9600 eV with a ion chamber as I0 detector and a Germanium 15 elements fluorescence detector, from Canberra Inc. The sample was placed in a flow-through reaction cell for in situ experiments. The absorption of a Cu foil was measured between a second and a third ion chambers before and after the in situ experiments. The X-ray fluorescence data was normalized by standard methods using the ATHENA software which is part of the IFFEFIT package[33] in order to obtain the normalized XANES spectra.

The NAP-XPS experiments were carried out at the CIRCE beamline of the ALBA synchrotron light source.[34] The acquisition was performed using a PHOIBOS 150 NAP electron energy analyzer (SPECS GmbH) equipped with four differential pumping stages and a set of electrostatic lenses which enable the performance of XPS measurements with the sample at pressures from ultrahigh vacuum (UHV, with a base pressure of 10^{-10} mbar) up to 20 mbar. Most of the experiments were performed at a chamber pressure of $1.5{\times}10^{-7}$ mbar, which we call High Vacuum (HV). All NAP-XPS measurements have been acquired with 1350 eV photon energy. XANES at the Cu-L_3 edge was also acquired at the same end station measured by Total Electron Yield (TEY). The current from the sample was amplified with a ALBA Em current amplifier and was normalized to the incident photon flux, measured via the Au-coated refocusing mirror. The spot size for both NAP-XPS and NEXAFS measurements was $\sim 100 \times 100$ μm^2. XANES techniques at the soft X-ray region are usually referred as Near Edge X-ray Absorption Fine Structure (NEXAFS), but we will maintain the XANES nomenclature to save acronyms that refer to the same physical phenomena.

Computational methods:
In all calculations on bare Cu_5 clusters, a trigonal bipyramidal (3D) structure is assumed. Although HOPG-supported Cu_5 clusters are used in the experiment, it has been previously shown[11] that these clusters are minimally perturbed by a carbon-based surface (graphene) due to the dispersion-dominated nature of the Cu_5–graphene interaction. Our theoretical approach combines Density functional theory (DFT) and multireference perturbation theory.[35] Due to the open-shell nature of the interacting species, the application of the multi-reference method has allowed to ensure the nature of the oxidation states of the copper atoms in Cu_5–$(O_2)_n$ complexes. The application of multireference perturbation theory has also allowed to determine the reaction pathways and the values of the energy barriers from physisorption to molecular chemisorption states, and to O_2 dissociation, as the wavefunction at these regions of the configurational space show a strong multiconfigurational character. The geometry optimizations of Cu_5–$(O_2)_n$ clusters geometries was performed at PBE-D3 level[20,36,21] given its excellent performance in describing supported and unsupported subnanometer silver[37,38] and copper[39,7] clusters. We used the atom-centered def2-TZVP[40] basis set for copper and oxygen atoms. The Helmholtz free energies of formation were calculated using the def2-QZVPP at the relaxed geometries, counterpoise-corrected, with the frequencies calculated with the def2-TZVP basis set. These calculations were realized with the `ORCA`[41] suite of programs (version 4.0.1.2). The chemical oxidation states of the copper atoms for each Cu_5–$(O_2)_n$ complex were deduced from an analysis of Mulliken charges[42] and atomic spin populations with the Hirshfeld method.[43,44] The optimized geometries calculated at DFT-D3 level were used as an initial guess in single-state internally-contracted RS2C[35] calculations with density fitting (DF-RS2C), as implemented within the `MOLPRO` program package.[45] The orbitals are first optimized using the single-state DF-CASSCF approach separately for the electronic states correlating with neutral and ionic fragments, using the `SUPER-CI` optimization method,[46] as implemented in a recent version of the `MOLPRO` code.[47] Next, the single-reference RS2C method is applied to correct for dynamical correlation effects. We used the polarized correlation-consistent triple-ζ basis of Dunning and collaborators[48] (cc-pVTZ) for oxygen atoms, and the cc-pVTZ-PP basis set for copper atoms[49] including a small (10-valence-electron) relativistic pseudopotential. For density fitting, the associated `MP2FIT` and `JKFIT` bases were used in CASSCF and RS2C calculations correspondingly.

Supporting Information

Supporting Information is available from the Wiley Online Library or from the author.

Acknowledgements

This research used resources of the Brazilian Synchrotron Light Laboratory (LNLS), an open national facility operated by the Brazilian Centre for Research in Energy and Materials (CNPEM) for the Brazilian Ministry for Science, Technology, Innovations and Communications (MCTIC). The XAFS2 beamline staff is acknowledged for the assistance during the experiments (proposals 20160754 and 20170907). The authors thank the support of ALBA staff for the successful performance of the measurements at CIRCE beamline (proposal 2018093158) of the ALBA Synchrotron Light Source. The STEM studies were performed at the DME-UCA node of the National Unique Infrastructure for Electron Microscopy of Materials, ELECMI. CESGA (Galicia, Spain) and CTI (CSIC) supercomputer centers are acknowledged for providing computational resources. **Funding:** This work has been partly

supported by the European Union's Horizon 2020 Research and Innovation Programme under Grant Agreement No. 825999; the Spanish Agencia Estatal de Investigación (AEI) and the Fondo Europeo de Desarrollo Regional (FEDER, UE) under Grant No. MAT2016-75354-P; the Austrian Science Fund (FWF) under Grant P29893-N36; the CMST COST Action CM1405 "Molecules in Motion" (MOLIM); the Xunta de Galicia, Spain (Grupos Ref. Comp. ED431C 2017/22 and AEMAT ED431E 2018/08); Obra Social Fundación La Caixa: Ref. LCF/PR/PR12/11070003; ANPCyT PICT (2017-1220 and 2017-3944) and UNLP (Project 11/X790), Argentina. **Data and materials availability:** All data needed to evaluate our conclusions are present in the main manuscript or the supplementary material.

Conflict of Interest

David Buceta and M.A. López-Quintela are stackholders of Nanogap, company dedicated to the exploitation of clusters, synthesized by wet chemical methods, in different fields (www.nanogap.es).

Credit authorship contribution statement

David Buceta, **Félix G. Requejo**, and **Manuel Arturo Lépez-Quintela** designed all the experimental work. S.H. and M.C. carried out the synthesis and characterization of clusters. **Giampaolo Barone** designed the initial structures of the Cu_5/O_2 adsorption complexes. **Giampaolo Barone** and **Héctor Lozano** carried out preliminary DFT analysis. **David Buceta**, **Carlos Escudero**, **Cristian Huck-Iriart**, **José M. Ramallo-López**, **Lisandro J. Giovanetti** and **Félix G. Requejo** planned all the synchrotron experiments. **David Buceta**, **Miguel Cuerva**, **Lisandro J. Giovanetti**, **José M. Ramallo-López**, **Cristian Huck-Iriart**, **Carlos Escudero** and **Félix G. Requejo** carried out the synchrotron measurements. **Juan Carlos Hernández**, **Jose Juán Calvino** and **Miguel López-Haro** carried out the STEM measurements and co-wrote the corresponding text. **María Pilar de Lara-Castells** coordinated all the theoretical and computational research presented, including its conceptualization. **Patricia López-Caballero**, **Alexander Zanchet**, **Alexander O. Mitrushchenkov**, **Andreas W. Hauser** and **María Pilar de Lara-Castells** performed the associated computer simulations, and analyzed the theoretical and computational data. **David Buceta** and **Manuel Arturo López-Quintela**. co-wrote the synthesis and characterization part of the main manuscript and the corresponding supplementary material. **Félix G. Requejo**, **Lisandro J. Giovanetti**, **Cristian Huck-Iriart**, and **José M. Ramallo-López** co-wrote the synchrotron part of the manuscript and the corresponding supplementary material. **Alexander Zanchet**, **Alexander O. Mitrushchenkov**, **Andreas W. Hauser** and **María Pilar de Lara-Castells** co-wrote the theoretical and computational part of the main manuscript and the corresponding supplementary material.

[1] P. Jena, Q. Sun, *Chem. Rev.* **2018**, *118,* 5755.

[2] M. Zhou, C. Zeng, Y. Chen, S. Zhao, M. Y. Sfeir, M. Zhu, R. Jin, *Nat. Comm.* **2016**, *7,* 13240.

[3] L. Liu, A. Corma, *Chem. Rev.* **2018**, *118,* 4981.

[4] P. Concepción, M. Boronat, S. García-García, E. Fernández, A. Corma, *ACS Catal.* **2017**, *7,* 3560.

[5] A. Halder, L. A. Curtiss, A. Fortunelli, S. Vajda, *J. Chem. Phys.* **2018**, *148,* 110901.

[6] S. Hirabayashi, M. Ichihashi, *Phys. Chem. Chem. Phys.* **2014**, *16,* 26500.

[7] P. López-Caballero, A. W. Hauser, M. P. de Lara-Castells, *J. Phys. Chem. C* **2019**, *123,* 23064.

[8] B. Yang, C. Liu, A. Halder, E. C. Tyo, A. B. F. Martinson, S. Seifert, P. Zapol, L. A. Curtiss, S. Vajda, *J. Phys. Chem. C* **2017**, *121,* 10406.

[9] P. Maity, S. Yamazoe, T. Tsukuda, *ACS Catal.* **2013**, *3,* 182.

[10] J. Oliver-Messeguer, L. Liu, S. García-García, C. Canós-Giménez, I. Domínguez, R. Gavara, A. Doménech-Carbó, P. Concepción, A. Leyva-Pérez, A. Corma, *J. Amer. Chem. Soc.* **2015**, *137,* 3894.

[11] M. P. de Lara-Castells, A. W. Hauser, J. M. Ramallo-López, D. Buceta, L. J. Giovanetti, M. A. López-Quintela, F. G. Requejo, *J. Mater. Chem. A* **2019**, *7,* 7489.

[12] A. L. Linsebigler, G. Q. Lu, J. T. Yates, Jr., *Chem. Rev.* **1995**, *95,* 735.

[13] E. C. Tyo, S. Vajda, *Nat. Nanotechnol.* **2015**, *10,* 577.

[14] S. Huseyinova, J. Blanco, F. G. Requejo, J. M. Ramallo-López, M. C. Blanco, D. Buceta, M. A. López-Quintela, *J. Phys. Chem. C* **2016**, *120,* 15902.

[15] E. Fernández, M. Boronat, A. Corma, *J. Phys. Chem. C* **2015**, *119,* 19832.

[16] A. Zanchet, P. López-Caballero, A. O. Mitrushchenkov, D. Buceta, M. A. López-Quintela, A. W. Hauser, M. P. de Lara-Castells, *J. Phys. Chem. C* **2019**, *123,* 27064.

[17] B. Eren, C. Heine, H. Bluhm, G. A. Somorjai, M. Salmeron, *J. Am. Chem. Soc.* **2015**, *137*, 34 11186.

[18] M. P. de Lara-Castells, J. L. Krause, *J. Chem. Phys.* **2003**, *118*, 11 5098.

[19] M. P. de Lara-Castells, A. O. Mitrushchenkov, O. Roncero, J. L. Krause, *Isr. J. Chem.* **2005**, *45*, 1–2 59.

[20] J. P. Perdew, K. Burke, M. Ernzerhof, *Phys. Rev. Lett.* **1996**, *77,* 3865.

[21] S. Grimme, S. Ehrlich, L. Goerigk, *J. Comp. Chem.* **2011**, *32,* 1456.

[22] A. W. Hauser, J. Gomes, M. Bajdich, M. Head-Gordon, A. T. Bell, *Phys. Chem. Chem. Phys.* **2013**, *15,* 20727.

[23] X. Yu, A. R. Oganov, Q. Zhu, F. Qi, G. Qian, *Phys. Chem. Chem. Phys.* **2018**, *20,* 30437.

[24] S. Bhattacharya, S. V. Levchenko, L. M. Ghiringhelli, M. Scheffler, *Phys. Rev. Lett.* **2013**, *111,* 135501.

[25] Y. Xu, W. A. Shelton, W. F. Schneider, *J. Phys. Chem. B* **2006**, *110,*, 33 16591.

[26] L. D. Landau, *Phys. Z. Sowjetunion* **1932**, *2,* 46.

[27] C. Zener, *Proc. R. Soc. London, Ser. A* **1932**, *137,* 696.

[28] A. W. Hauser, M. P. de Lara-Castells, *J. Phys. Chem. Lett.* **2016**, *7* 4929.

[29] L. Liu, M. Lopez-Haro, C. W. Lopes, C. Li, P. Concepcion, L. Simonelli, J. J. Calvino, A. Corma, *Nat. Mater.* **2019**, *18,* 866.

[30] E. J. Kirkland, *Advanced Computing in Electron Microscopy*, Springer US, **2010**.

[31] S. Bernal, F. Botana, J. Calvino, C. López-Cartes, J. Pérez-Omil, J. Rodríguez-Izquierdo, *Ultramicroscopy* **1998**, *72,* 135 .

[32] S. J. A. Figueroa, J. C. Mauricio, J. Murari, D. B. Beniz, J. R. Piton, H. H. Slepicka, M. F. de Sousa, A. M. Espíndola, A. P. S. Levinsky, *J. Phys. Conf. Ser.* **2016**, *712,* 012022.

[33] B. Ravel, M. Newville, *J. Synchrotron Radiat.* **2005**, *12*, 4 537.

[34] V. Pérez-Dieste, L. Aballe, S. Ferrer, J. Nicolàs, C. Escudero, A. Milán, E. Pellegrin, *J. Phys. Conf. Ser.* **2013**, *425,* 072023.

[35] P. Celani, H.-J. Werner, *J. Chem. Phys.* **2000**, *112,* 5546.

[36] S. Grimme, J. Antony, S. Ehrlich, H. Krieg, *J. Chem. Phys.* **2010**, *132,* 154104.

[37] M. P. de Lara-Castells, C. Cabrillo, D. A. Micha, A. O. Mitrushchenkov, T. Vazhappilly, *Phys. Chem. Chem. Phys.* **2018**, *20,* 19110.

[38] P. López-Caballero, J. M. Ramallo-López, L. J. Giovanetti, D. Buceta, S. Miret-Artés, M. A. López-Quintela, F. G. Requejo, M. P. de Lara-Castells, *J. Mater. Chem. A* **2020**, *8,* 6842.

[39] S. Huseyinova, J. Blanco, F. G. Requejo, J. M. Ramallo-López, M. C. Blanco, D. Buceta, M. A. López-Quintela, *J. Phys. Chem. C* **2016**, *120,* 15902.

[40] F. Weigend, R. Ahlrichs, *Phys. Chem. Chem. Phys.* **2005**, *7,* 3297.

[41] F. Neese, *Wiley Interdiscip. Rev. Comput. Mol. Sci.* **2018**, *8,* e1327.

[42] R. S. Mulliken, *J. Chem. Phys.* **1962**, *36,* 3428.

[43] F. L. Hirshfeld, *Theor. Chim. Acta* **1977**, *44,* 129.

[44] P. Bultinck, C. Van Alsenoy, P. W. Ayers, R. Carbó-Dorca, *J. Chem. Phys.* **2007**, *126,* 144111.

[45] H. J. Werner, P. J. Knowles, G. Knizia, F. R. Manby, M. Schütz, P. Celani, T. Korona, R. Lindh, A. O. Mitrushchenkov, G. Rauhut, et al., Molpro, the most recent version, a package of ab initio programs, see http://www.molpro.net, **2018**.

[46] D. A. Kreplin, P. J. Knowles, H.-J. Werner, *J. Chem. Phys.* **2019**, *150,* 194106.

[47] H.-J. Werner, P. J. Knowles, F. R. Manby, J. A. Black, K. Doll, A. Heßelmann, D. Kats, A. Köhn, T. Korona, D. A. Kreplin, Q. Ma, T. F. Miller, A. Mitrushchenkov, K. A. Peterson, I. Polyak, G. Rauhut, M. Sibaev, *J. Chem. Phys.* **2020**, *152,* 144107.

[48] D. E. Woon, T. H. Dunning, Jr., *J. Chem. Phys.* **1994**, *100,* 2975.

[49] D. Figgen, G. Rauhut, M. Dolg, H. Stoll, *Chem. Phys.* **2005**, *311,* 227.

Table of Contents

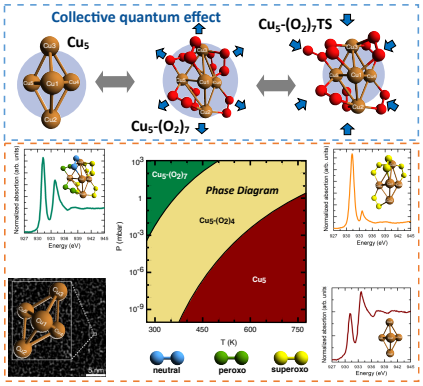

ToC Entry: Cu_5 clusters display nobility at a broad range of temperatures and oxygen pressures. It arises from an unusual reversible oxidation which is observed by in situ X-ray Absorption Spectroscopy and X-ray Photoelectron Spectroscopy. Collective quantum effects, featured by subnanometer-sized metal clusters, are responsible of the observed nobility.